

Hybrid Spin-Crossover Complexes

Supramolecular Interaction Tuning of Spin-Crossover in Pyrene/Fullerene (C₆₀) Tethered Fe^{II}-2,6-Di(pyrazol-1-yl)pyridine Complexes: Towards Switchable Molecular DevicesKuppusamy Senthil Kumar,^{*[a]} Ivan Šalitroš,^[b,c] Nithin Suryadevara,^[d]
Eufemio Moreno-Pineda,^[d] and Mario Ruben^{*[a,d]}

Abstract: A set of functional SCO systems based on Fe^{II}-2,6-di(pyrazol-1-yl)pyridine (BPP), Fe^{II}-BPP, featuring supramolecular pyrene and fullerene (C₆₀) anchoring groups for nanocarbon materials are designed and synthesized. The pyrene tethered complexes [Fe(L¹)₂](BF₄)₂ and [Fe(L²)₂](BF₄)₂ comprise structurally different BPP-pyrene ligand systems L¹ (BPP-COOR, R = -CH₂-pyrene) and L² [BPP-CH₂OR, R = -OC(CH₂)-pyrene]. The [Fe(L¹)₂](BF₄)₂ complex showed gradual and high temperature SCO (T_{1/2} = ca. 450 K), whereas the [Fe(L²)₂](BF₄)₂ complex re-

mained trapped in the high spin (HS) state in the 300–5 K temperature range. On the other hand, the bulky fullerene (C₆₀) tethered complex, [Fe(L³)₂](BF₄)₂, is HS at 385 K and showed gradual but incomplete SCO, upon cooling, centered at 208 K. The results compiled in this study indicate the dominant role of intermolecular interactions in tuning/blocking SCO in the studied Fe^{II}-BPP complexes, a fact that needs to be carefully weighed while designing functional-SCO systems.

Introduction

Design and synthesis of functional molecular materials are at the forefront of materials chemistry research due to their diverse applicability, especially in nanotechnology and molecular electronics/spintronics.^[1] Spin-crossover (SCO) based materials^[1–6] capable of undergoing cooperative hence abrupt SCO behavior are promising candidates for the realization of molecular electronics/spintronics components.^[2,7] Designing SCO complexes with an additional physical function such as luminescence, thus functional-SCO complex,^[8] is of paramount importance towards realizing SCO based applications. For e.g. the luminescent moiety tethered SCO complex^[9,10] can be modulated and probed by light-photons, a faster way of signal processing at the molecular scale. On the other hand, the realization of novel SCO active functional-hybrid materials such as graphene-SCO hybrid^[11–13] requires chemical tethering of the SCO

core with aromatic anchoring groups such as pyrene/fullerene (C₆₀). The pyrene/fullerene (C₆₀) groups enable non-covalent anchoring of an SCO complex on the graphene surface. The non-covalent functionalization of graphene is highly desired because it preserves, except for the molecule induced doping, the electronic structure of the graphene.^[14] Most importantly, the graphene-SCO hybrid material is desirable for applications due to the conducting nature of the graphene and bistable magnetic characteristics of the SCO complexes. The conductance characteristics of the resultant graphene-SCO hybrid could be externally and reversibly manipulated by controlling the spin state of the anchored SCO complex. For e.g. via light-induced excited spin state trapping (LIEEST)^[15,16] effect. However, the afore-described deliberate chemical tethering of a parent SCO complex core with a functional addend leads to altered spin state switching characteristics of the resultant functional-SCO system relative to its parent entity. This is due to the sensitive nature of the SCO even to the slightest of changes in structural parameters. In this context, our group is actively involved in the design, synthesis, and structure-property elucidation of SCO active materials in bulk and at molecular dimensions resulting in several important results.^[17,18] For e.g. we have recently reported spin-state dependent conductance switching in few-layer graphene (FLG)-SCO junctions.^[18] To develop further in this direction and to understand the role of chemical functionalization in tuning the SCO characteristics, a set of Fe^{II}-SCO complexes based on the prototypical 2,6-di(pyrazol-1-yl)pyridine (BPP) ligand system^[19–22] is rationally designed and their SCO characteristics are probed.

The complexes feature supramolecular pyrene/fullerene (C₆₀) anchoring groups^[23–26] (L¹–L³, cf. Scheme 1) to enable the development of SCO active nanocarbon hybrid materials.^[27–29]

[a] Institut de Physique et Chimie des Matériaux de Strasbourg (IPCMS), CNRS-Université de Strasbourg, 23, rue du Loess, BP 43, 67034 Strasbourg cedex 2, France
E-mail: senthil.kuppusamy@ipcms.unistra.fr
http://www.ipcms.unistra.fr/?page_id=11816

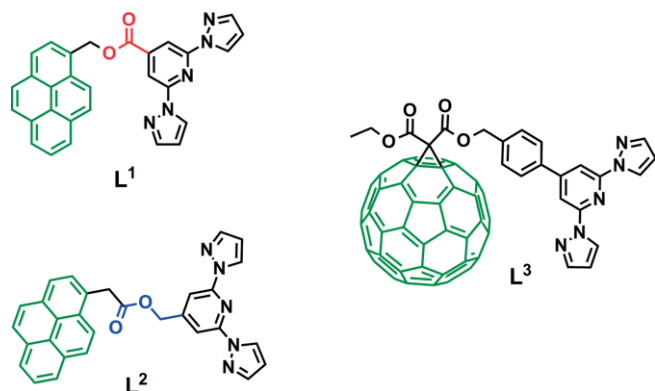
[b] Institute of Inorganic Chemistry, Technology and Materials, Faculty of Chemical and Food Technology, Slovak University of Technology, Bratislava, 81237, Slovak Republic

[c] Central European Institute of Technology, Brno University of Technology, Purkynova 123, 612 00 Brno, Czech Republic

[d] Institute of Nanotechnology, Karlsruhe Institute of Technology (KIT), Hermann-von-Helmholtz-Platz 1, 76344, Eggenstein-Leopoldshafen, Germany
E-mail: Mario.ruben@kit.edu
<https://www.ruben-group.de/home.html>

Supporting information and ORCID(s) from the author(s) for this article are available on the WWW under <https://doi.org/10.1002/ejic.201801109>.

The pyrene tethered complexes detailed in this study are suitable candidates to probe spin-state dependence of electronic transport in single SCO complex junctions employing FLG electrodes.^[18] The short spacers associated with the pyrene-based systems discussed in this study, relative to the previously reported pyrene-BPP systems featuring comparatively longer spacers,^[30,31] are useful models to understand the role of spacer length in altering SCO characteristics. The spacer length varia-



Scheme 1. The pyrene (L^1 and L^2) and fullerene (L^3) tethered BPP ligand systems used to prepare functional-SCO complexes reported in this study. The bulky substituents are shown in green, whereas the red and blue colored parts indicate differing nature of the linkage between pyrene and BPP moieties in L^1 and L^2 .

tion could also enable a programmable distance scaling between the SCO core and FLG electrode altering the mechanistic aspects of electron transport^[32] in FLG-SCO complex junctions.

The fullerene (C_{60}) tethered ligand system (L^3) is designed in view of the advantageous electronic properties and better anchoring abilities associated with fullerene (C_{60}) in molecular junctions.^[24,25] Further, the fullerene-based complex also serves as a model system complementing our recent report detailing transport in SCO-FLG junctions.^[18] In the following sections, structure-property relations associated with the Fe^{II} -BPP complexes featuring ligands L^1 - L^3 are discussed.

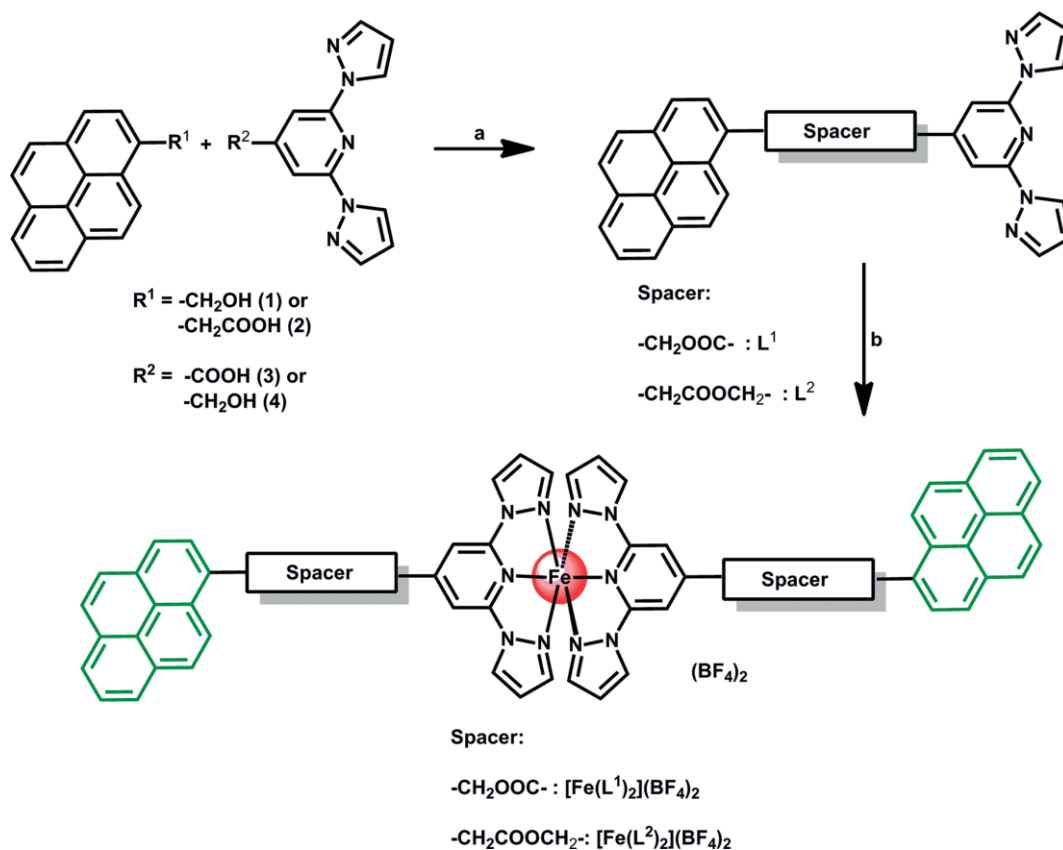
Results and Discussion

Synthesis of the Ligands and Complexes

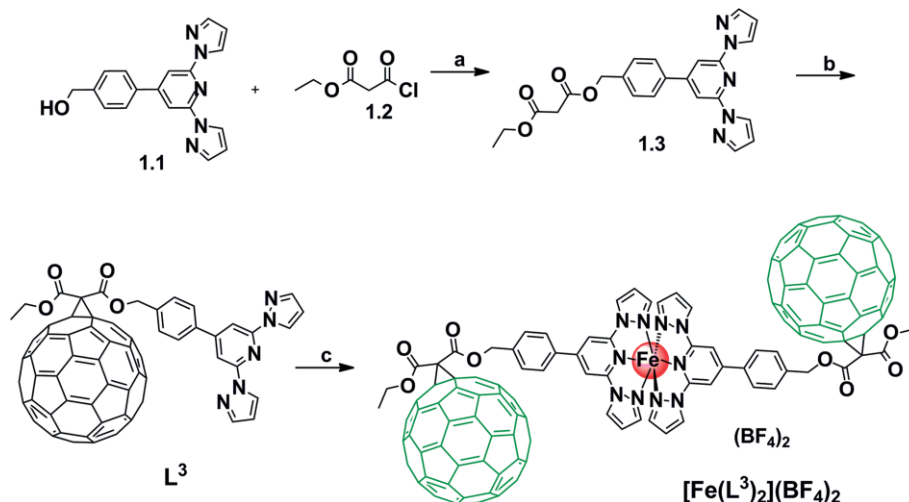
The syntheses of the ligands L^1 and L^2 were carried out via *N,N*-dicyclohexylcarbodiimide (DCC) coupling reactions between the corresponding pyrene and BPP derivatives as depicted in Scheme 2.

The target Fe^{II} complexes $[Fe(L^1)_2](BF_4)_2$ and $[Fe(L^2)_2](BF_4)_2$ were synthesized by performing complexation reactions in $CH_2Cl_2/MeOH$ solvent mixture.

A standard Bingel reaction^[33] between the malonyl-BPP derivative 1.3 (cf. Scheme 3) and the fullerene yielded ligand L^3 as methanofullerene adduct which upon complexation with Fe^{II}



Scheme 2. Syntheses of pyrene decorated SCO modules. Key: (a) DCC/DMAP, DCM, room temp., Ar, 24 h, yield: 47 % for L^1 and 57 % for L^2 and (b) $Fe(BF_4)_2 \cdot 6H_2O$, $CH_2Cl_2/MeOH$, r.t., Ar, 4 h, yield: 52 % for $[Fe(L^1)_2](BF_4)_2$ and 58 % for $[Fe(L^2)_2](BF_4)_2$.



Scheme 3. Syntheses of fullerene decorated SCO module. Key: (a) Pyridine, DCM, room temp., Ar, 24 h, (b) DBU, toluene, Ar, 5 h, and (c) $\text{Fe}(\text{BF}_4)_2 \cdot 6\text{H}_2\text{O}$, DCM/THF, r.t., Ar, 4 h, yield: 21 %. See experimental section for further details.

ions yielded the expected complex as a highly insoluble brown precipitate.

Photophysical Properties of the Ligands and Complexes

Photophysical properties of the pyrene tethered ligands and complexes were measured in 1:1 dichloromethane (DCM)/acetonitrile (ACN) binary solvent mixture. The rationale behind choosing such solvent system is to ensure solubility of the ligands and complexes in a medium of the same polarity to make meaningful comparisons. The UV/Vis spectral features of the pyrene substituted ligands and Fe^{II} complexes depicted in Figure S1 and S2 showed the expected pyrene-based electronic transitions in line with the previous reports.^[34] Upon excitation of the pyrene-based $S_2 \leftarrow S_0$ band located at 343 nm, the ligands and complexes showed characteristic pyrene-based luminescence centered around 373 nm (cf. Figure S1 and S2). The UV/Vis absorbance characteristics of the fullerene substituted ligand L^3 in DCM solvent showed the expected fullerene-based bands typical of a methanofullerene derivative (cf. Figure S3). The probing of photophysical characteristics of the corresponding complex $[\text{Fe}(L^3)_2](\text{BF}_4)_2$ in solution is proved to be impossible due to the highly insoluble nature of the complex and its susceptibility to sonication inducing complex disassociation.

Magnetic Properties of the Complexes

Variable temperature magnetic investigations of the reported complexes are focused on the detection and characterization of the photo- or thermally activated SCO phenomena (cf. Figure 1 and Figure 2). The complex $[\text{Fe}(L^1)_2](\text{BF}_4)_2$ with a shorter $-\text{CH}_2\text{OOC}-$ spacer separating the pyrene anchoring group and SCO core (cf. Scheme 2) showed gradual and high-temperature SCO (Figure 1, black circles). At 450 K, the χT value of ca. $2.41 \text{ cm}^3 \text{ K mol}^{-1}$ was obtained indicating approximately 70 % of the complexes in the HS state. Above 450 K, the decomposition of the complex took place making it impossible to reach

the HS state plateau prohibiting the determination of the exact $T_{1/2}$ temperature. For photomagnetic experiments, the complex $[\text{Fe}(L^1)_2](\text{BF}_4)_2$ was prepared as a thin layer to ensure light pene-

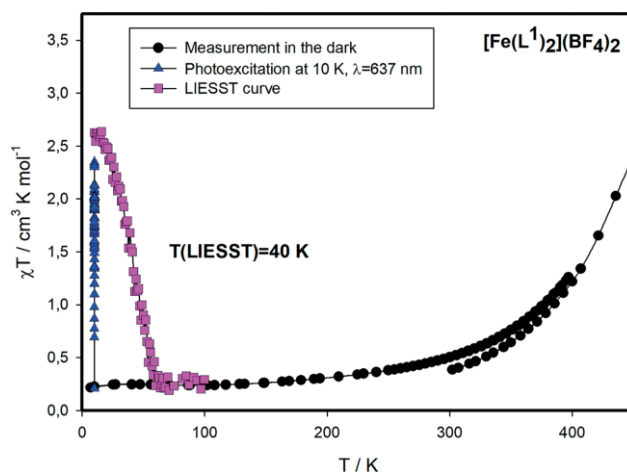


Figure 1. (a) χT vs. T plot and photomagnetic characteristics of $[\text{Fe}(L^1)_2](\text{BF}_4)_2$.

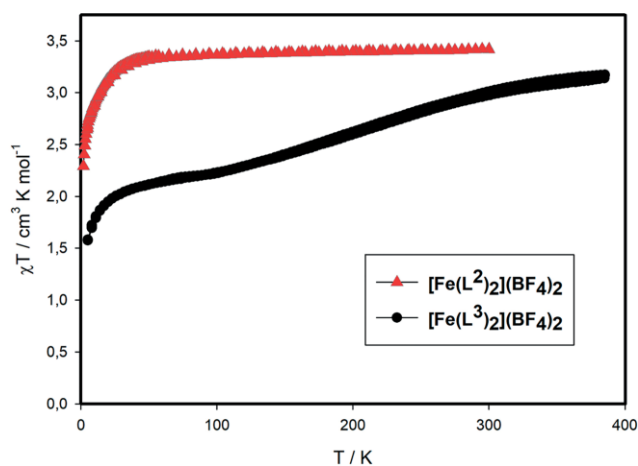


Figure 2. χT vs. T plots of $[\text{Fe}(L^2)_2](\text{BF}_4)_2$ and $[\text{Fe}(L^3)_2](\text{BF}_4)_2$.

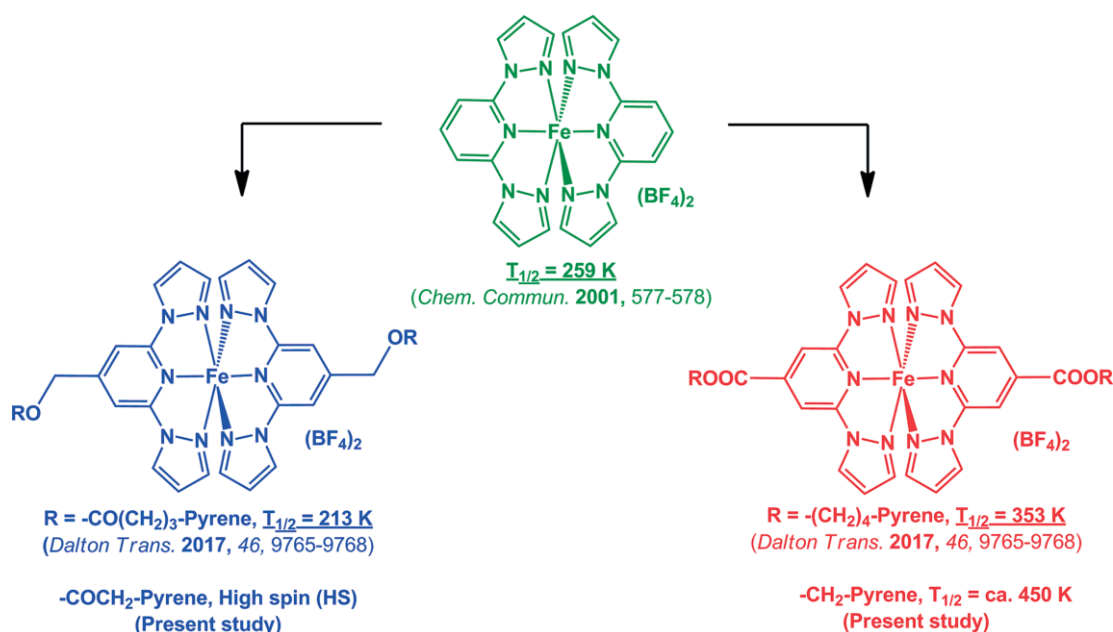
tration upon irradiation. At 10 K, where the complex is in LS state, the light irradiation ($\lambda = 637$ nm or 532 nm, 10 mW cm^{-2}) caused a significant increase of magnetic signal. The red-light photoexcitation ($\lambda = 637$ nm) was found to be more efficient (Figure 1, blue triangles). Consecutive measurement in the dark allowed studying variable temperature magnetic properties of the metastable HS state (Figure 1, pink squares). The maximum of χT vs. T product was at ca. $2.5 \text{ cm}^3 \text{ K mol}^{-1}$ which corresponds to about 80 % material in HS state. The $T(\text{LIESST})$ value calculated from the minimum in the $\partial(\chi T)/\partial T$ vs. T curve is 40 K. The relaxation of metastable HS fraction upon the increase of temperature (LIESST curve) of the $[\text{Fe}(\text{L}^1)_2](\text{BF}_4)_2$ showed a rather non-cooperative character, as it is anticipated from the gradual shape of thermally induced SCO curves.^[35]

The χT vs. T plot of the $[\text{Fe}(\text{L}^2)_2](\text{BF}_4)_2$ complex (Figure 2, red triangles) showed that system is in HS state at 300 K. The χT value of ca. $3.40 \text{ cm}^3 \text{ mol}^{-1} \text{ K}$ is in the expected range for HS iron(II) mononuclear complexes. The low temperature decrease of the χT product function is attributed to the zero-field splitting effect.

The complex $[\text{Fe}(\text{L}^3)_2](\text{BF}_4)_2$ (Figure 2, black circles) exhibits gradual and incomplete SCO, upon cooling from 385 K ($\chi T = 3.13 \text{ cm}^3 \text{ mol}^{-1} \text{ K}$), centered at 208 K. The values of the χT function in the LS region (< 100 K) indicate that about 50 % of compound is frozen in the remnant HS state.

The present study is important in terms of realizing functional SCO complexes, especially with supramolecular anchoring groups for the noncovalent functionalization of nanocarbon materials. The differences in the SCO characteristics between the pyrene tethered complexes $[\text{Fe}(\text{L}^1)_2](\text{BF}_4)_2$ and $[\text{Fe}(\text{L}^2)_2](\text{BF}_4)_2$ are ascribed to electronic and steric effects originating from variations in ligand field around Fe^{II} and strong intermolecular interactions operating between the grafted substituents around the switching core, respectively. The LS nature of the

$[\text{Fe}(\text{L}^1)_2](\text{BF}_4)_2$ complex at 300 K is tentatively attributed to the increased π -acidic nature of the ligand L^1 facilitating metal to ligand ($d-\pi^*$) back-bonding interaction as detailed in the literature for Fe^{II} -BPP complexes.^[36,30] In contrast, the absence of such interaction in $[\text{Fe}(\text{L}^2)_2](\text{BF}_4)_2$ complex (see Scheme 1 for ligand structures) rendered the system HS at 300 K in accordance with our previous reports.^[30] However, contrary to their congeners showing complete spin state switching,^[30] the SCO characteristics of $[\text{Fe}(\text{L}^1)_2](\text{BF}_4)_2$ and $[\text{Fe}(\text{L}^2)_2](\text{BF}_4)_2$ complexes are totally different: the $[\text{Fe}(\text{L}^2)_2](\text{BF}_4)_2$ complex is trapped in its HS state, whereas the $[\text{Fe}(\text{L}^1)_2](\text{BF}_4)_2$ complex showed very gradual SCO with $T_{1/2}$ situated around 450 K. A legitimate hypothesis explaining this observation would be the steric hindrance-mediated blocking of the SCO due to the pyrene group-mediated $\pi-\pi$ interactions operating around the switching centers. The blocking would then be imposed by the tight packing of the complexes facilitating strong intermolecular contacts especially amongst pyrene entities. These intermolecular contacts hinder the SCO to occur or attain completion, as reported from our group for the crystal structure of a similar but structurally rigid pyrene tethered Fe^{II} -BPP complex.^[31] Such steric constraints are absent in the previously studied pyrene tethered complexes, featuring relatively longer spacers which added flexibility to the system and hence the volume expansion upon SCO is better accommodated in the lattice. The above points clearly elucidate the nature/role of chemical substitution/spacer in determining the intramolecular electronic and intermolecular steric interactions in modulating SCO characteristics which are going hand in hand in determining spin-state switching characteristics. A similar blocked SCO characteristic, i.e., incomplete HS to LS conversion, observed in $[\text{Fe}(\text{L}^3)_2](\text{BF}_4)_2$ complex, featuring a bulky fullerene (C_{60}) anchoring group through a short spacer, further implies the role of intermolecular steric interactions in blocking SCO.



Scheme 4. Comparison between the SCO characteristics of the parent complex (green) with the pyrene decorated complexes. The complexes featuring $-\text{CH}_2\text{OR}$ and $-\text{COOR}$ functional addends are depicted in blue and red colors, respectively.

To get further insights into the role of spacer groups and pyrene anchoring groups, the SCO characteristics of the pyrene tethered complexes discussed in this and previous study^[30] are compared with the parent complex, $[\text{Fe}(\text{BPP})_2](\text{BF}_4)_2$, reported by Halcrow and co-workers.^[19] The parent complex showed abrupt first order SCO with a $T_{1/2} = 259$ K and a ca. 3 K thermal hysteresis loop. Interestingly, the pyrene tethered complexes featuring a $-\text{CH}_2\text{OR}$ type spacer between the BPP core and pyrene anchoring group showed either SCO around 213 K or trapped in the HS state (cf. Scheme 4, blue color-coded complexes).

On the contrary, the Fe^{II}-BPP complexes featuring a $-\text{COOR}$ type spacer between the BPP core and pyrene anchoring group showed above room temp. SCO as detailed in Scheme 4, red color-coded complexes. Overall, the SCO became more gradual in the substituted complexes relative to the parent complex. This indicates the role of pyrene groups in blocking cooperative interactions between the switching Fe-BPP core via intermolecular interactions. A clear proof for this conclusion is the more gradual and blocked SCO characteristics observed for the Fe^{II} complexes featuring relatively short spacers reported in this study.

Conclusions

A set of functional SCO complexes based on the Fe^{II}-BPP core are designed, synthesized, and their magnetic properties are investigated to elucidate the role of chemical functionalization mediated tuning of SCO characteristics. The short nature of spacers between Fe^{II}-BPP core and pyrene groups in the $[\text{Fe}(\text{L}^1)_2](\text{BF}_4)_2$ and $[\text{Fe}(\text{L}^2)_2](\text{BF}_4)_2$ complexes proved to be a hindrance to spin-state switching, a facet also observed in a complex featuring bulky fullerene group. This study underscores the delicate adjustment of intermolecular interactions required for the elaboration of such spin-state switching complexes. Moreover, the insoluble nature of the fullerene-based complexes proved to be a difficulty towards processing it in terms of applications. This indicates that the emphasis should be more on the judicious choice of spacer/solubilizing groups to confer solution processability. Further, the pyrene and fullerene anchoring groups tethered far away from the switching Fe^{II}-BPP core exerted no electronic effect over the ligand field parameters of the BPP ligand skeleton. Only steric effects are observed which proved to be a bottle neck in realizing SCO. Despite these shortcomings, the SCO complexes detailed in this study could be a useful stepping stone to develop molecular materials and devices with novel functions. For example, in view of the reports detailing self-assembly of pristine fullerene^[37] and its derivatives^[38,39] leading to the observation of exotic nanostructured materials, SCO nanostructures could be obtained by synthesizing a judiciously designed fullerene-SCO system.

Experimental Section

Materials and Methods: Anhydrous solvents and $\text{Fe}(\text{BF}_4)_2 \cdot 6\text{H}_2\text{O}$ were purchased from commercial sources and used as received. Glassware was dried in a vacuum oven at 150 °C prior to the experi-

ments. All the reactions were performed under argon (Ar) atmosphere unless otherwise noted. UV/Vis absorption spectral measurements were performed with a Varian Cary 5000 double-beam UV/Vis-NIR spectrometer. Solution and solid phase PL measurements were performed on a Photon Technology International (PTI) spectrometer at ambient temperature. All herein reported magnetic measurements were performed on an MPMS-XL7 or MPMS-XL5 SQUID magnetometer (Quantum Design). For standard magnetic measurement in the dark, the temperature dependent magnetization was recorded at an applied magnetic field (B_{DC}) of 0.1 T. The temperature sweeping rate was 1 K min^{-1} for the cooling and heating scans. Gelatin capsule (standard measurements in the dark) was used as sample holders in the temperature range 5 \leftrightarrow 400 K. The very small diamagnetic contribution of the gelatin capsule had a negligible contribution to the overall magnetization which was dominated by the sample. In the case of high-temperature magnetic measurement (300–450 K), the experiment was carried out using a special heating setup. High-temperature sample holder consisted of Quartz glass tube and Teflon filler. The diamagnetic corrections of the molar magnetic susceptibilities were applied using Pascal's constants. The photomagnetic measurements were performed using a diode-pumped solid-state lasers (DPSS) Kvant ($\lambda = 637$ nm or 532 nm, 300 mW) coupled through an optical fiber to the cavity of an MPMS SQUID and the power on the sample surface was adjusted to 10 mW cm^{-2} . For the photomagnetic experiments, a small amount of sample was introduced onto transparent tape and mounted into the sample holder. The exact weight of samples (ca 0.1 mg) was obtained by weighing and verified by comparison of thermal $\chi_m T$ vs. T curve with that of a more accurately weighed sample of the same compound. After the cooling to 10 K, the sample, now in the low spin state was irradiated and the change in magnetization was followed. When the saturation point had been reached (after ca. 300 min), the light was switched off, the temperature was increased at a rate of 0.3 K min^{-1} , and the magnetization was measured at 1 K intervals. $T(\text{LIESST})$ value was determined from the minimum of the $\partial(\chi T)/\partial T$ vs. T curve for the relaxation process.

Synthesis of the Ligands and Complexes

Synthesis of 2,6-Di-pyrazol-1-yl-isonicotinic Acid Pyren-1-yl-methylester (L^1): An oven dried 25 mL Schlenk flask with a stir bar was charged with 4-pyrenemethanol (**1**) (0.232 g, 1 mmol) and 2,6-di(1*H*-pyrazol-1-yl)isonicotinic acid **3** (0.255 g, 1 mmol) and the solids placed under Argon atmosphere. To this, anhydrous CH_2Cl_2 (20 mL) was added and the mixture cooled to 0 °C in an Ice-Water bath. DCC (0.206 g, 1 mmol) and DMAP (0.122 g, 1 mmol) were then added to the stirring mixture slowly as solids and slowly allowed to attain r.t. and stirred for 24 h. The reaction mixture was filtered, and the filtrate was washed with water twice and the organic layer was dried with standing on Na_2SO_4 . Purification was accomplished by silica gel column chromatography using 9:1 $\text{CH}_2\text{Cl}_2/\text{CH}_3\text{OH}$ as an eluent. L^1 was obtained as a half-white powder. Yield: 0.220 g (47 %). $^1\text{H NMR}$ (300 MHz, CDCl_3 , 300 K, TMS): $\delta = 8.503\text{--}8.494$ (d, 2 H), 8.403–8.395 (m, 3 H), 8.225–7.988 (m, 8 H), 7.739 (s, 2 H), 6.48–6.466 (t, 2 H), 6.166 (s, 2 H) ppm. $^{13}\text{C NMR}$ (75 MHz, CDCl_3 , 300 K, TMS): 66.284, 108.337, 109.224, 122.56, 124.641, 124.874, 125.532, 125.609, 126.074, 127.136, 127.314, 127.859, 127.976, 128.063, 128.514, 129.696, 130.645, 131.150, 131.990, 142.753, 143.171, 150.709, 164.061. ESI-MS ($\text{CH}_2\text{Cl}_2/\text{CH}_3\text{OH}$): $m/z = 492.1403$ [$\text{M} + \text{Na}$]⁺. $\text{C}_{29}\text{H}_{19}\text{N}_5\text{O}_2 \cdot 0.45 \cdot \text{CH}_3\text{OH}$ (501.05): calcd. C 73.1, H 4.33, N 14.47; found C 73.08, H 4.06, N 14.32.

Synthesis of $[\text{Fe}(\text{L}^1)_2](\text{BF}_4)_2$: L^1 (0.094 g, 0.2 mmol) was added to 20 mL of dry DCM under Ar and stirred until complete solubilization of ligand occurred. To this $\text{Fe}(\text{BF}_4)_2 \cdot 6\text{H}_2\text{O}$ (0.03375 g, 0.1 mmol) in

1 mL of MeOH was added. The deep red solution was stirred at room temp. for 4 h. Solvents were evaporated under reduced pressure and the dark red solid was dissolved in minimum amount of acetonitrile and kept for crystallization by slowly diffusing Et₂O. Analytically pure title complex was obtained as microcrystalline solid after 1–2 weeks' time. Yield: 62 mg (52 %). ESI-MS (CH₃CN): *m/z* = 497.1218 [Fe(L¹)₂]²⁺. C₅₈H₃₈N₁₀O₄FeB₂F₈·H₂O (1186.05): calcd. C 58.71, H 3.4, N 11.81; found C 58.65, H 3.62, N 12. IR (KBr): $\tilde{\nu}$ = 3438, 3040, 1734, 1630, 1575, 1527, 1499, 1474, 1462, 1408, 1249, 1052, 971, 841, 763, 598, 520 and 418 cm⁻¹.

Synthesis of Pyren-1-yl-acetic Acid 2,6-Di-pyrazol-1-yl-pyridin-4-ylmethylester (L²): An oven dried 25 mL Schlenk flask with a stir bar was charged with 4-pyrene acetic acid **2** (0.26 g, 1 mmol) and [2,6-di(1*H*-pyrazol-1-yl)pyridin-4-yl]methanol **4** (0.241 g, 1 mmol) and the solids placed under Argon atmosphere. To this, anhydrous CH₂Cl₂ (20 mL) was added and the mixture cooled to 0 °C in an Ice-Water bath. DCC (0.206 g, 1 mmol) and DMAP (0.122 g, 1 mmol) were then added to the stirring mixture slowly as solids and slowly allowed to attain r.t. and stirred for 24 h. The reaction mixture was filtered, and the filtrate was washed with water twice and the organic layer was dried with standing on Na₂SO₄. Purification was accomplished by silica gel column chromatography using CH₂Cl₂ as an eluent and the product was recrystallized from hexane to yield L² as white powder in analytically pure form. Yield: 0.278 g (57 %). ¹H NMR (300 MHz, CDCl₃, 300 K, TMS): δ = 8.5 (d, 2 H), 8.3 (d, 2 H), 8.18 (m, 8 H), 7.7 (s, 2 H), 7.6 (s, 2 H), 6.4 (s, 2 H), 5.2 (s, 2 H), 4.4 (s, 2 H) ppm. ¹³C NMR (75 MHz, CDCl₃, 300 K, TMS): 66.284, 108.337, 109.224, 122.56, 124.641, 124.874, 125.532, 125.609, 126.074, 127.136, 127.314, 127.859, 127.976, 128.063, 128.514, 129.696, 130.645, 131.150, 131.990, 142.753, 143.171, 150.709, 164.061. ESI-MS (CH₂Cl₂/CH₃OH): *m/z* = 484.18 [M + H]⁺. C₃₀H₂₁N₅O₂ (483.53): calcd. C 74.52, H 4.38, N 14.48; found C 74.23, H 4.72, N 14.34.

Synthesis of [Fe(L²)₂](BF₄)₂: L² (0.097 g, 0.2 mmol) was added to 20 mL of dry DCM under Ar and stirred until complete solubilization of ligand occurred. To this Fe(BF₄)₂·6H₂O (0.034 g, 0.1 mmol) in 1 mL of MeOH was added. The yellow solution was stirred at room temp. for 4 h. Solvents were evaporated under reduced pressure and the solid was dissolved in minimum amount of acetonitrile and kept for crystallization by slowly diffusing Et₂O. Analytically pure title complex was obtained as microcrystalline solid after 1–2 weeks' time. Yield: 69 mg (58 %). ESI-MS (CH₃CN): *m/z* = 511.44 [Fe(L²)₂]²⁺. C₆₀H₄₂B₂F₈FeN₁₀O₄ (1196.51): calcd. C 60.23, H 3.54, N 11.71; found C 59.99, H 3.73, N 11.75. IR (KBr): $\tilde{\nu}$ = 3453, 3120, 1736, 1634, 1581, 1527, 1464, 1407, 1337, 1276, 1211, 1055, 971, 851, 770, 711, 601, 519 and 424 cm⁻¹.

Synthesis of 4-[2,6-Di(1*H*-pyrazol-1-yl)pyridin-4-yl]benzyl Ethylmalonate (1.3): To an ice cold solution of 106 mg (0.33 mmol) of {4-[2,6-di(1*H*-pyrazol-1-yl)pyridin-4-yl]phenyl}methanol in dry dichloromethane, 50 μ L (0.33 mmol) of ethyl 3-chloro-3-oxopropanoate was added along with two equivalents of pyridine 52 μ L (0.66 mmol) under Argon atmosphere and stirred overnight. The solvent was evaporated and the crude mixture was packed on a silica gel column and eluted with 7:3 ethyl acetate/hexane mixture to yield the title compound as a waxy solid. Yield: 61.5 mg. ¹H NMR (500 MHz, CDCl₃, 300 K, TMS): δ = 8.575–8.570 (d, *J* = 2.5 Hz, 2 H, pyrazole), 8.069 (s, 2 H, Pyridine), 7.796–7.779 (d, *J* = 8.5 Hz, 2 H, phenyl), 7.761–7.758 (d, *J* = 1.5 Hz, 2 H, pyrazole), 7.479–7.462 (d, *J* = 8.5 Hz, 2 H, phenyl), 6.491–6.482 (q, 2 H, pyrazole), 5.239 (s, 2 H, COO-CH₂), 4.226–4.184 (q, 2 H, COO-CH₂), 3.452 (s, 2 H, COCH₂CO), 1.271–1.242 (t, 3 H, CH₃). ESI-TOF MS (Da): *m/z* (rel. intensity, assigned structure) 432.1633 (100 %, C₂₃H₂₁N₅O₄ + H⁺, Calc. 432.1666).

Synthesis of C₆₀-BPP Ligand (L³): DBU (28.8 μ L) was added under Argon at room temp. to a stirred solution of C₆₀ (71 mg, 0.1 mmol), 4-[2,6-di(1*H*-pyrazol-1-yl)pyridin-4-yl]benzyl ethyl malonate (43.12 mg, 0.1 mmol) and Iodine (23.58 mg, 0.1 mmol) in toluene (75 mL). The resulting solution was stirred under Argon at room temp. for 5 h. The solvent was evaporated, and the crude mixture was packed on a silica gel column and eluted with 10 % CS₂ in hexane to remove the unreacted fullerene. Further elution with dichloromethane and 5 % MeOH in dichloromethane yielded the C₆₀-BPP Ligand (L³) as dark brown solid. Yield: 60 mg (52 %). ¹H NMR (500 MHz, CDCl₃, 300 K, TMS): δ = 8.628–8.623 (d, *J* = 2.5 Hz, 2 H, pyrazole), 8.125 (s, 2 H, Pyridine), 7.875–7.858 (d, *J* = 8.5 Hz, 2 H, phenyl), 7.801–7.799 (d, *J* = 1 Hz, 2 H, pyrazole), 7.671–7.655 (d, *J* = 8 Hz, 2 H, phenyl), 6.54–6.532 (q, 2 H, pyrazole), 5.601 (s, 2 H, COO-CH₂), 4.553–4.51 (q, 2 H, COO-CH₂), 1.427–1.339 (t, 3 H, CH₃). ESI-TOF MS (Da): *m/z* (rel. intensity, assigned structure) 1150.1224 (100 %, C₈₃H₁₉N₅O₄ + H⁺, Calc. 1150.1510).

Synthesis of [Fe(L³)₂](BF₄)₂: To a 0.05 mmol (57.45 mg) of C₆₀-BPP ligand (L³) in 50 mL of dry and degassed DCM, 0.025 mmol (8.437 mg) of Fe(BF₄)₂·6H₂O in 1 mL of dry THF was added under Ar protection leading to immediate precipitate formation, the reaction mixture was stirred for 4 h. The precipitate was washed with cold THF and DCM, note the ligand is highly soluble in DCM and THF solvents. Yield: 0.013 g (21 %). C₁₆₆H₃₈B₂F₈FeN₁₀O₈·CH₂Cl₂ (2614.06): calcd. C 76.72, H 1.54, N 5.36; found C 76.51, H 1.80, N 5.21.

Acknowledgments

Grant Agencies [France: Innovation FRC: Self-assembly of spin crossover (SCO) complexes on graphene; Slovakia: APVV-14-0078, APVV-14-0073, VEGA 1/0125/18] are acknowledged for the financial support. This research has been financially supported by the Ministry of Education, Youth and Sports of the Czech Republic under the project CEITEC 2020 (LQ1601).

Keywords: Iron · Spin-crossover · Anchoring groups · Functional materials · Molecular electronics

- [1] K. S. Kumar, M. Ruben, *Coord. Chem. Rev.* **2017**, *346*, 176–205.
- [2] M. A. Halcrow (Ed.), *Spin-Crossover Materials Properties and Applications*, John Wiley & Sons, Ltd, **2013**.
- [3] P. Gütllich, Y. Garcia, H. A. Goodwin, *Chem. Soc. Rev.* **2000**, *29*, 419–427.
- [4] O. Kahn, *Science* **1998**, *279*, 44–48.
- [5] E. Collet, P. Guionneau, *Comptes Rendus Chim.* **2018** (In press).
- [6] E. Breuning, M. Ruben, J.-M. Lehn, F. Renz, Y. Garcia, V. Ksenofontov, P. Gütllich, E. Wegelius, K. Rissanen, *Angew. Chem. Int. Ed.* **2000**, *39*, 2504–2507; *Angew. Chem.* **2000**, *112*, 2563–2566.
- [7] B. Weber, W. Bauer, J. Obel, *Angew. Chem. Int. Ed.* **2008**, *47*, 10098–10101; *Angew. Chem.* **2008**, *120*, 10252.
- [8] K. S. Kumar, M. Studniarek, B. Heinrich, J. Arabski, G. Schmerber, M. Bowen, S. Boukari, E. Beaurepaire, J. Dreiser, M. Ruben, *Adv. Mater.* **2018**, *30*, 1705416.
- [9] C. Lochenie, K. Schötz, F. Panzer, H. Kurz, B. Maier, F. Puchtl, S. Agarwal, A. Köhler, B. Weber, *J. Am. Chem. Soc.* **2018**, *140*, 700–709.
- [10] C.-F. Wang, G.-Y. Yang, Z.-S. Yao, J. Tao, *Chem. Eur. J.* **2018**, *24*, 3218–3224.
- [11] K. S. Kumar, I. Šalitroš, Z. Boubegeten-Fezoua, S. Moldovan, P. Hellwig, M. Ruben, *Dalton Trans.* **2018**, *47*, 35–40.
- [12] D. Qiu, D.-H. Ren, L. Gu, X.-L. Sun, T.-T. Qu, Z.-G. Gu, Z. Li, *RSC Adv.* **2014**, *4*, 31323–31327.
- [13] Y. Murashima, M. R. Karim, N. Saigo, H. Takehira, R. Ohtani, M. Nakamura, M. Koinuma, L. F. Lindoy, K. Kuroiwa, S. Hayami, *Inorg. Chem. Front.* **2015**, *2*, 886–892.

- [14] S. Decurtins, P. Gütllich, C. P. Kçhler, H. Spiering, A. Hauser, *Chem. Phys. Lett.* **1984**, *105*, 1–4.
- [15] A. Hauser, P. Gütllich, H. Spiering, *Inorg. Chem.* **1986**, *25*, 4245–4248
- [16] V. Georgakilas, M. Otyepka, A. B. Bourlinos, V. Chandra, N. Kim, K. C. Kemp, P. Hobza, R. Zboril, K. S. Kim, *Chem. Rev.* **2012**, *112*, 6156–6214.
- [17] E. J. Devid, P. N. Martinho, M. V. Kamalakar, I. Šalitroš, Ú. Prendergast, J.-F. Dayen, V. Meded, T. Lemma, R. González-Prieto, F. Evers, T. E. Keyes, M. Ruben, B. Doudin, S. J. van der Molen, *ACS Nano* **2015**, *9*, 4496–4507.
- [18] E. Burzuri Linares, A. García-Fuente, V. García-Suárez, K. S. Kumar, M. Ruben, J. Ferrer, H. S. J. van der Zant, *Nanoscale* **2018**, *10*, 7905–7911.
- [19] J. M. Holland, C. A. Kilner, M. Thornton-Pett, M. A. Halcrow, J. A. McAllister, Z. Lu, *Chem. Commun.* **2001**, 577–578.
- [20] M. A. Halcrow, *Coord. Chem. Rev.* **2005**, *249*, 2880–2908.
- [21] M. A. Halcrow, *New J. Chem.* **2014**, *38*, 1868–1882.
- [22] M. A. Halcrow, *Coord. Chem. Rev.* **2009**, *253*, 2493–2514.
- [23] S. Kyatskaya, J. R. Galán Mascarós, L. Bogani, F. Hennrich, M. Kappes, W. Wernsdorfer, M. Ruben, *J. Am. Chem. Soc.* **2009**, *131*, 15143–15151.
- [24] T. M. Figueira-Duarte, K. Müllen, *Chem. Rev.* **2011**, *111*, 7260–7314.
- [25] S. Bailey, D. Visontai, C. J. Lambert, M. R. Bryce, H. Frampton, D. Chappell, *J. Chem. Phys.* **2014**, *140*, 054708.
- [26] C. A. Martin, D. Ding, J. K. Sørensen, T. Bjørnholm, J. M. van Ruitenbeek, H. S. J. van der Zant, *J. Am. Chem. Soc.* **2008**, *130*, 13198–13199.
- [27] E. Nuin, W. Bauer, A. Hirsch, *Eur. J. Org. Chem.* **2017**, *2017*, 790–798.
- [28] J. Dugay, M. Aarts, M. Giménez-Marqués, T. Kozlova, H. W. Zandbergen, E. Coronado, H. S. J. van der Zant, *Nano Lett.* **2017**, *17*, 186–193.
- [29] D. V. Konarev, S. S. Khasanov, A. F. Shestakov, M. Ishikawa, A. Otsuka, H. Yamochi, G. Saito, R. N. Lyubovskaya, *J. Am. Chem. Soc.* **2016**, *138*, 16592–16595.
- [30] K. S. Kumar, I. Šalitroš, E. Moreno-Pineda, M. Ruben, *Dalton Trans.* **2017**, *46*, 9765.
- [31] R. González-Prieto, B. Fleury, F. Schramm, G. Zoppellaro, R. Chandrasekar, O. Fuhr, S. Lebedkin, M. Kappes, M. Ruben, *Dalton Trans.* **2011**, *40*, 7564–7570.
- [32] N. J. Tao, *Nat. Nanotechnol.* **2006**, *1*, 173–181.
- [33] C. Bingel, *Chem. Ber.* **1993**, *126*, 1957–1959.
- [34] A. G. Crawford, A. D. Dwyer, Z. Liu, A. Steffen, A. Beeby, L.-O. Pålsson, D. J. Tozer, T. B. Marder, *J. Am. Chem. Soc.* **2011**, *133*, 13349–13362.
- [35] J. Klingele, D. Kaase, M. Schmucker, Y. Lan, G. Chastanet, J.-F. Létard, *Inorg. Chem.* **2013**, *52*, 6000–6010.
- [36] L. J. Kershaw Cook, R. Kulmaczewski, R. Mohammed, S. Dudley, S. A. Barrett, M. A. Little, R. J. Deeth, M. A. Halcrow, *Angew. Chem. Int. Ed.* **2016**, *55*, 4327–4331; *Angew. Chem.* **2016**, *128*, 4399.
- [37] M. Sathish, K. Miyazawa, *J. Am. Chem. Soc.* **2007**, *129*, 13816–13817.
- [38] T. Nakanishi, *Chem. Commun.* **2010**, *46*, 3425–3436.
- [39] K. S. Kumar, A. Patnaik, *Langmuir* **2011**, *27*, 11017–11025.

Received: September 17, 2018